SANDIA REPORT
SAND2014-15576
Unlimited Release
Printed July 2014

Guidelines for Effective Radiation Transport for Cable SGEMP Modeling Part I: X-Ray Environments

Clifton R. Drumm, Wesley C. Fan and C. David Turner

Prepared by
Sandia National Laboratories
Albuquerque, New Mexico 87185 and Livermore, California 94550

Sandia National Laboratories is a multi-program laboratory managed and operated by Sandia Corporation, a wholly owned subsidiary of Lockheed Martin Corporation, for the U.S. Department of Energy's National Nuclear Security Administration under contract DE-AC04-94AL85000.

Sandia National Laboratories

Issued by Sandia National Laboratories, operated for the United States Department of Energy by Sandia Corporation.

Available to DOE and DOE contractors from
U.S. Department of Energy
Office of Scientific and Technical Information
P.O. Box 62
Oak Ridge, TN 37831

Telephone: (865) 576-8401
Facsimile: (865) 576-5728
E-Mail: reports@adonis.osti.gov
Online ordering: http://www.osti.gov/bridge

Available to the public from
U.S. Department of Commerce
National Technical Information Service
5285 Port Royal Rd.
Springfield, VA 22161

Telephone: (800) 553-6847
Facsimile: (703) 605-6900
E-Mail: orders@ntis.fedworld.gov
Online order: http://www.ntis.gov/help/ordermethods.asp?loc=7-4-0#online

SAND2014-15576
Unlimited Release
Printed July 2014

Guidelines for Effective Radiation Transport for Cable SGEMP Modeling Part I: X-Ray Environments

Clifton R. Drumm and Wesley C. Fan
Department 01341 Radiation Effects Theory

C. David Turner
Department 01352 Electromagnetic Theory

Sandia National Laboratories
P. O. Box 5800
Albuquerque, New Mexico 87185-1179

Abstract

This report describes experiences gained in performing radiation transport computations with the SCEPTRE radiation transport code for System Generated ElectroMagnetic Pulse (SGEMP) applications. SCEPTRE is a complex code requiring a fairly sophisticated user to run the code effectively, so this report provides guidance for analysts interested in performing these types of calculations. One challenge in modeling coupled photon/electron transport for SGEMP is to provide a spatial mesh that is sufficiently resolved to accurately model surface charge emission and charge deposition near material interfaces. The method that has been most commonly used to date to compute cable SGEMP typically requires a sub-micron mesh size near material interfaces, which may be difficult for meshing software to provide for complex geometries. We present here an alternative method for computing cable SGEMP that appears to substantially relax this requirement. The report also investigates the effect of refining the energy mesh and increasing the order of the angular approximation to provide some guidance on determining reasonable parameters for the energy/angular approximation needed for x-ray environments. Conclusions for γ-ray environments may be quite different and will be treated in a subsequent report. In the course of the energy-mesh refinement studies, a bug in the cross-section generation software was discovered that may cause under prediction of the result by as much as an order of magnitude for the test problem studied here, when the electron energy group widths are much smaller than those for the photons. Results will be presented and compared using cross sections generated before and after the fix. We also describe adjoint modeling, which provides sensitivity of the total charge drive to the source energy and angle of incidence, which is quite useful for comparing the effect of changing the source environment and for determining most stressing angle of incidence and source energy. This report focusses on cable SGEMP applications, but many of the conclusions will be directly applicable for box Internal ElectroMagnetic Pulse (IEMP) modeling as well.

CONTENTS

FIGURES

TABLE

1. INTRODUCTION

The purpose of this report is to summarize and consolidate experiences gained using the SCEPTRE radiation transport code (Pautz, 2009) for modeling cable System-Generated ElectroMagnetic Pulse (SGEMP). The role of SCEPTRE is to model the transport of photons from an x-ray or γ-ray source within a cable and to track the electrons generated by various mechanisms, including Compton scattering and the photoelectric effect. The data from SCEPTRE, e.g. surface electron emissions, charge deposition distribution and electron current distribution, are handed off to the Emphasis code for ElectroMagnetics (EM) modeling (Turner, 2005), (Turner, 2011). The SCEPTRE calculations are performed in steady-state, so that time-integrated values are handed off to Emphasis, which then models the time dependence of the circuit response. The time scale of the photon/electron transport is assumed to be fast compared with the time response of the electrical circuit, so that performing the radiation transport in steady state is a good approximation.

SCEPTRE is a large and complex code so that effective use of the code requires some experience to avoid inaccurate or erroneous results from the code or inefficient use. It is hoped that this report will help analysts to avoid some pitfalls in using the code and to provide a jumpstart in running the code effectively and efficiently. Although this investigation is primarily concerned with cable SGEMP analyses, much of the information presented here is equally applicable to box Internal ElectroMagnetic Pulse (IEMP) modeling as well. Modeling of an x-ray source is covered in this report, and γ-ray modeling, which may be quite different due to differences in the cross sections, will be covered in a subsequent report.

One of the major difficulties in performing radiation transport for SGEMP analyses is to provide a spatial mesh that is sufficiently resolved near material interfaces so that spatial errors do not overwhelm the solution. It has been common for x-ray environments to need a sub-μm sized mesh, or even sub tenth-of-a-μm mesh near material interfaces. We have been investigating an alternative method that appears to substantially relax this requirement. Currently SGEMP is computed by combining the knock-on charge component from surface emission with the induced-charge component from the charge-deposition distribution. An alternative approach that computes SGEMP from the electron current distribution (Shockley, 1938) appears to provide accurate results with a much coarser mesh. The two methods are mathematically equivalent but numerically quite different for a coarse spatial mesh. The alternative method currently does not allow for including Radiation Induced Conductivity (RIC) in the EM modeling, but it may be possible to include an approximate RIC model as a perturbation. The two methods will be described and compared later in this report.

We also provide some guidance and results for refining the energy mesh and angular quadrature order to help the analyst to set up parameters for these variables. In the course of this work a bug was discovered in the CEPXS code (Lorence, 1989), which is used to generate photon/electron cross sections. The bug may lead to inaccurate results if the electron energy group widths are much smaller than the photon group widths. The effect of the bug on SGEMP modeling and the bug fix will be documented here.

Finally, we provide some guidance and results for performing adjoint SGEMP modeling (Renken, 1977). An adjoint calculation essentially proceeds backwards from response to source, providing a wealth of information, including the SGEMP response for all source energies and angles of incidence in a single calculation. Adjoint modeling is extremely useful for determining sensitivity of the SGEMP response to the source energy and for determining the most stressing angle-of-incidence of the source photons.

2. DESCRIPTION OF TEST CABLE

The test problem used for these analyses is the rg402 solid shield coaxial cable, which is a low-response cable in x-ray environments. The center conductor is silver-coated, copper-coated iron, and the outer shield is copper. The cable dimensions and materials are shown in Table 1, and a sketch of a typical solid-shield coaxial cable is shown in Fig. 1. The SCEPTRE modeling is performed in two-dimensional geometry, and the results are normalized per unit length of the cable.

Table 1. rg402 solid shield coaxial cable materials and dimensions

Material	Outer radius (cm)
Iron	0.0478
Copper	0.0594
Silver	0.0606
PTFE	0.15113
copper	0.17907

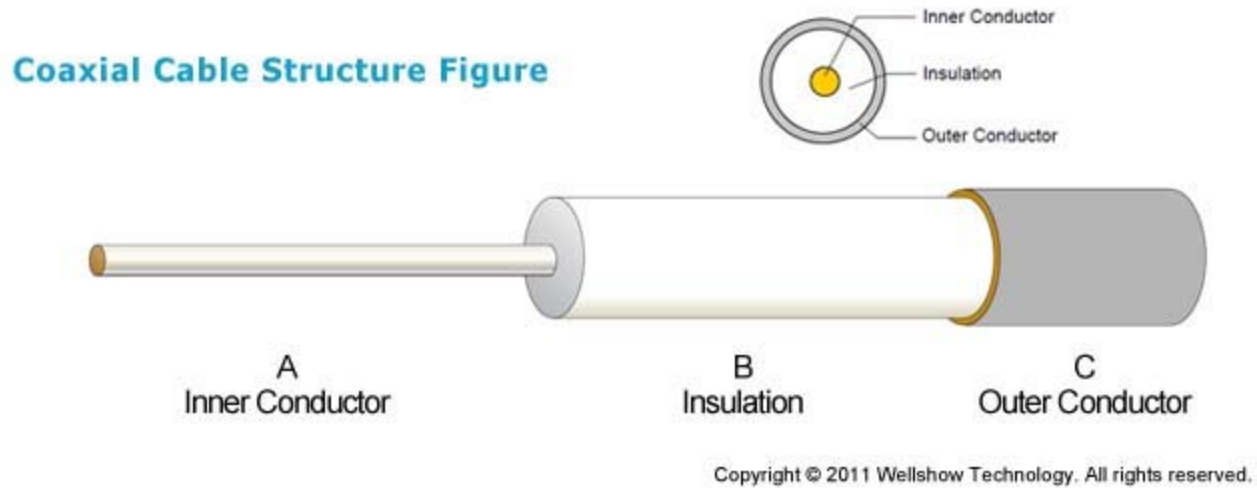

Figure 1. Solid-shield coaxial cable.

For these analyses, the outer conductor is grounded and a load is applied to the center conductor. The SGEMP direct-drive current is accumulated from a number of sources, 1) electrons knocked off of the outer ground into the dielectric and electrons displaced within the dielectric that produce an induced charge, 2) electrons knocked off of the inner conductor that produce a knock-on charge, and 3) electrons knocked off of the inner conductor and deposited in the dielectric that contribute to the induced charge.

It is important to consider the cable materials when setting up the energy mesh for the model, as will be described in detail later in this report, e.g. the silver K-edge is at about 25.5 keV, where there is a large jump in the attenuation coefficient, so it is desirable to include an edge in the energy mesh at 25.5 keV.

3. PITHON SOURCE X-RAY ENVIRONMENT

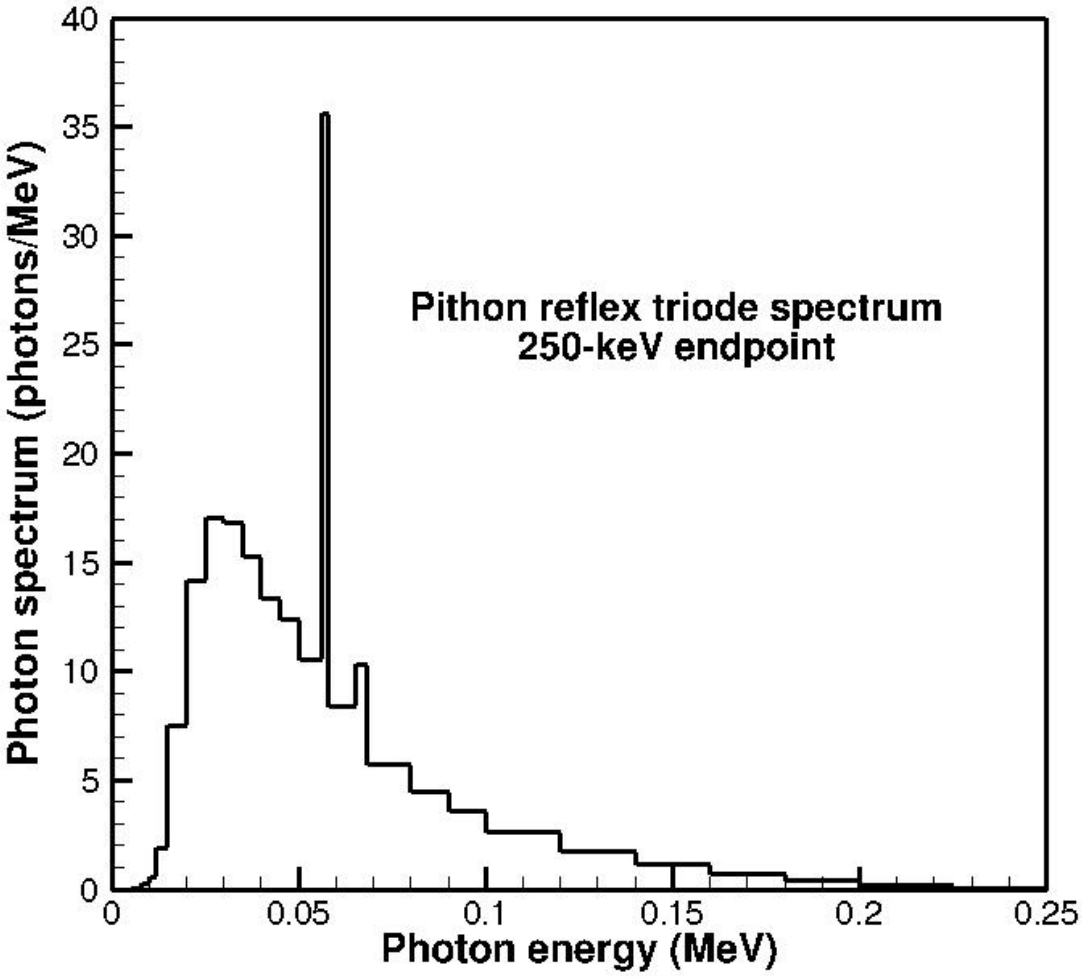

Figure 2. Pithon 250-keV endpoint photon spectrum.

The starting point of the calculations is a 250-keV endpoint Pithon x-ray source spectrum provided by L-3 Communications (Riordan), shown in Fig. 2. The results are normalized to 1 kRad(CaF_2) ThermoLuminescence Detector (TLD) dose. The normalization is determined from a one-dimensional model of a TLD, equilibrated with 1 mil aluminum. The dose profile for the 250-keV Pithon spectrum on an equilibrated 35-mil TLD is shown in Fig. 3.

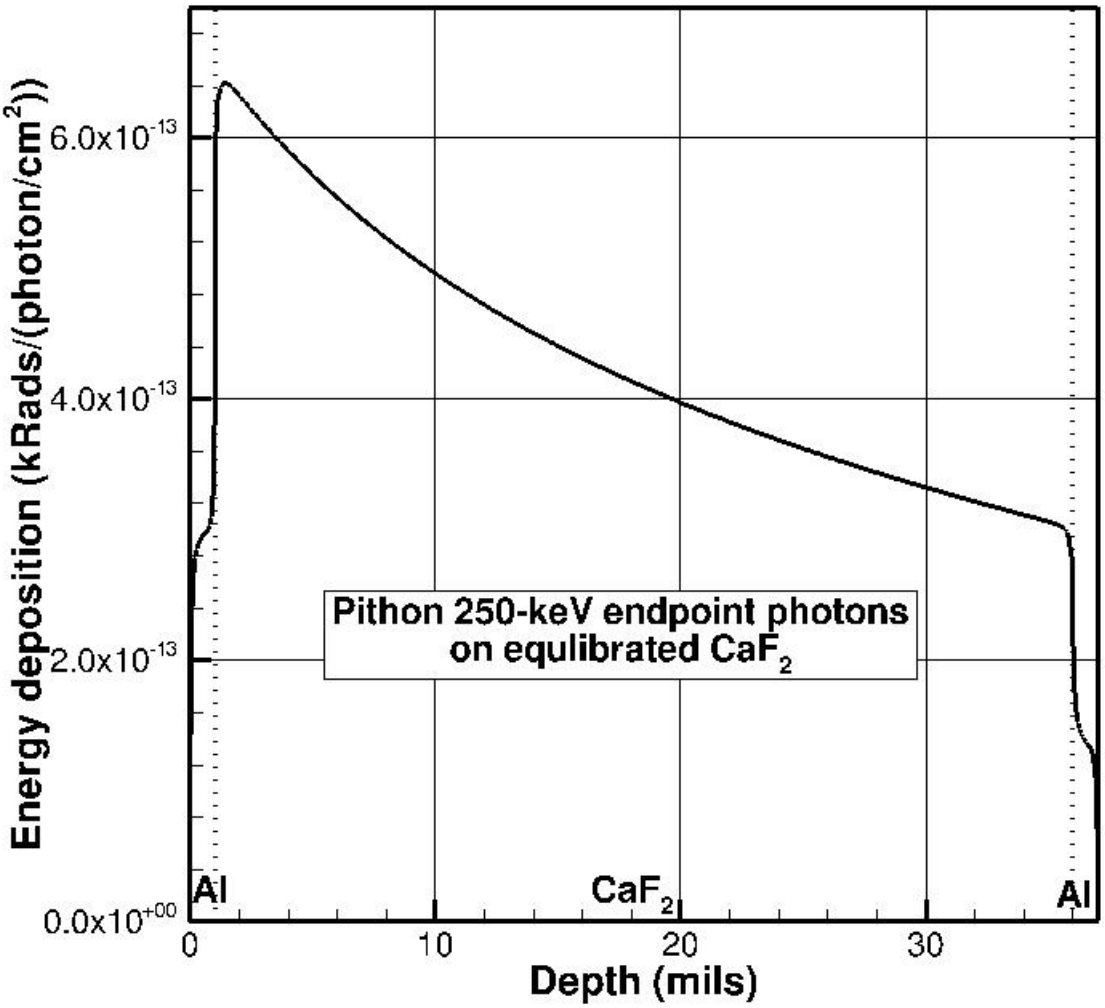

Figure 3. Normalization of source to CaF_2 TLD.

4. SGEMP MODELING OVERVIEW

Cable SGEMP direct drive current is generated by two mechanisms: 1) electrons that are directly knocked onto the center conductor, and 2) electrons that are induced on the center conductor by charge deposited in the surrounding dielectric material. The knock-on charge component is

$$q_{ko} = \oint \mathbf{J}_\beta(\mathbf{r}) \cdot d\mathbf{s} \qquad (4.1)$$

where $\mathbf{J}_\beta(\mathbf{r})$ is the electron current distribution vector and the integral is performed over the dielectric-conductor interface. $d\mathbf{s}$ is an element of surface area directed inwardly. SCEPTRE computes the electron angular flux distribution, ψ_β, as a function of space $\mathbf{r}$, angle $\mathbf{\Omega}$, and energy E over the entire phase space, and the electron current vector is computed from the electron angular flux by

$$\mathbf{J}_\beta(\mathbf{r}) = \int_{E_{cut}}^{E_{upper}} \int_{4\pi} \mathbf{\Omega}\psi_\beta(\mathbf{r}, \mathbf{\Omega}, E) d\mathbf{\Omega} dE \qquad (4.2)$$

where E_{cut} is the lower-energy cutoff of the electron cross sections and E_{upper} is the upper energy, $\mathbf{\Omega}$ is the particle direction vector and the angular integral is carried out over a unit sphere. The induced charge is given by (Shockley, 1938)

$$q_i = -\int V(\mathbf{r})\rho(\mathbf{r}) d\mathbf{r} \qquad (4.3)$$

where V($\mathbf{r}$) is a potential function, which is the solution to the Laplace equation, with boundary conditions of unity on the center conductor and zero on the outer ground

$$\nabla^2 V(\mathbf{r}) = 0 \qquad (4.4)$$

and $\rho(\mathbf{r})$ is the charge density. $\rho(\mathbf{r})$ is related to the electron current by

$$\rho(\mathbf{r}) = -\nabla \cdot \mathbf{J}_\beta(\mathbf{r}) \qquad (4.5)$$

The net direct-drive charge is the difference between the knock-on charge and the induced charge,

$$q_{net} = q_{ko} - q_i = \oint \mathbf{J}_\beta(\mathbf{r}) \cdot d\mathbf{s} + \int V(\mathbf{r})\rho(\mathbf{r}) d\mathbf{r} \qquad (4.6)$$

Experience has shown that computing the net charge in this manner, by separately computing the knock-on and induced components, and combining the results, is numerically very inaccurate unless an extremely fine spatial mesh is used near the dielectric-conductor interface. There are a couple of reasons for this. First, the gradient in the electron flux is extremely steep near material interfaces due to a large number of short range electrons being knocked off of the higher-Z material into the lower-Z material. For this reason, accurately computing the knock-on component of the charge requires a fine spatial mesh. Second, knock-on and induced components of the charge generally are similar in magnitude, so that the net charge is a small difference between two larger values, so that errors in either the knock-on component or induced component are magnified when taking the difference.

An alternative method for computing the total direct-drive charge is presented here (Drumm, Scrivner, & Hohlfelder, 1991), and preliminary results indicate that the alternative method

produces accurate results for a much coarser spatial mesh than by using Eq. (4.6). By substituting the expression for the charge density from Eq. (4.5) into Eq. (4.3) and applying the divergence theorem, the induced charge may be written

$$q_i = \int V(\mathbf{r}) \bigtriangledown \cdot \mathbf{J}_\beta(\mathbf{r}) d\mathbf{r} = -\int \bigtriangledown V(\mathbf{r}) \cdot \mathbf{J}_\beta(\mathbf{r}) d\mathbf{r} + \oint \mathbf{J}_\beta(\mathbf{r}) \cdot d\mathbf{s} \quad (4.7)$$

Substituting this expression for the induced charge into Eq. (4.6) results in this simpler expression for the net charge

$$q_{net} = q_{ko} - q_i = \int \bigtriangledown \mathbf{V}(\mathbf{r}) \cdot \mathbf{J}_\beta(\mathbf{r}) d\mathbf{r} = -\int \vec{\mathcal{E}}(\mathbf{r}) \cdot \mathbf{J}_\beta(\mathbf{r}) d\mathbf{r} \quad (4.8)$$

where $\mathcal{E}(\mathbf{r})$ is an electric field vector that is related to the potential function by

$$\vec{\mathcal{E}}(\mathbf{r}) = -\bigtriangledown V(\mathbf{r}) \quad (4.9)$$

Using this alternative formulation, the net charge no longer depends directly on the knock-on charge or a small difference between two larger quantities, but becomes a function of the electron current vector distribution in the dielectric. Preliminary results indicate that this alternative formulation provides accurate results using a much coarser mesh than using Eq. (4.6) directly. The next section will present results comparing the spatial truncation errors of the two methods.

5. SPATIAL MESH REFINEMENT

Using SCEPTRE/Emphasis to model cable SGEMP requires that the analyst provide a spatial mesh that is adequately refined to model the electron transport accurately. A useful starting point in determining meshing parameters is to perform a one-dimensional radiation transport calculation using the source spectrum, to reveal the electron charge distributions near material interfaces. Fig. 4 shows the result of a one-dimensional transport calculation, showing the charge deposition distribution in the vicinity of the silver layer in the rg402 on a μm-size scale. Fig. 4 indicates that a μm- or sub μm-size mesh will be needed, especially near the silver-PTFE interface, while a coarse mesh would be adequate away from material interfaces.

Generating a μm-sized mesh for the entire problem geometry is usually unreasonable, e.g. for this rg402, the simplest of cable geometries, about 10 million elements would be required for a μm-size mesh everywhere. Alternatively, using a very-fine mesh near material interfaces and transitioning to a coarse mesh away from interfaces may result in elements with poor quality and large aspect ratios, in extreme cases generating elements with near zero or negative Jacobians that cause instabilities in the transport calculation.

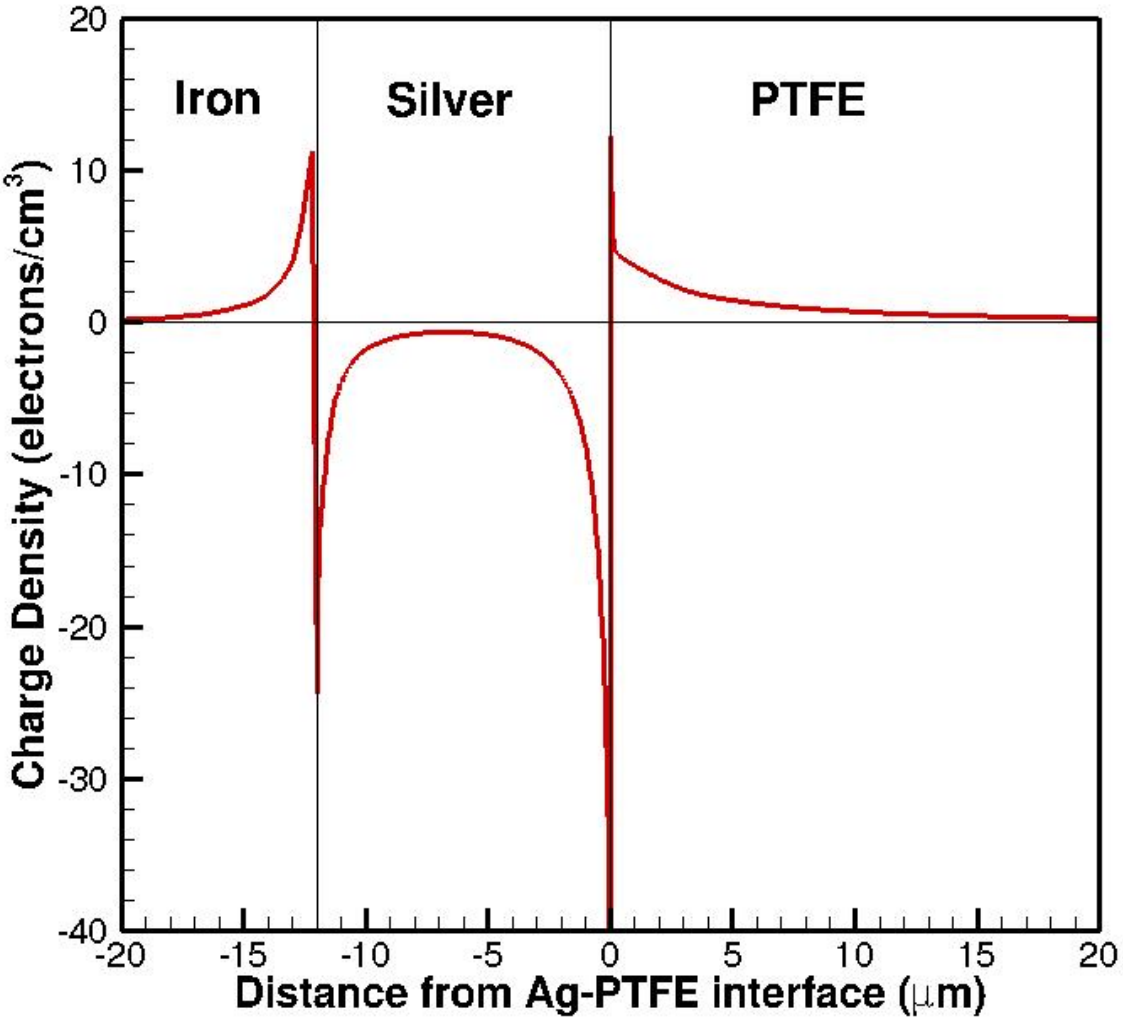

Figure 4. Charge deposition profile near silver layer in rg402 coax.

Generating an optimal spatial mesh is somewhat of an art, providing sufficient refinement in "important" parts of the geometry for accuracy, while being coarse enough in "unimportant" parts of the geometry for efficiency. Since the characteristic transport lengths of the photons are much longer than those of the electrons, the mesh refinement is driven by the electron transport, not the photon transport. Fig. 5 shows a baseline mesh of the rg402 coax, with element size of 8 μm normal to the dielectric/conductor interfaces. This particular mesh has aspect ratio values up to about 10, which occurs in the mesh near the silver/PTFE interface. Further study is needed to determine the effect of large aspect-ratio elements on the radiation transport and EM modeling.

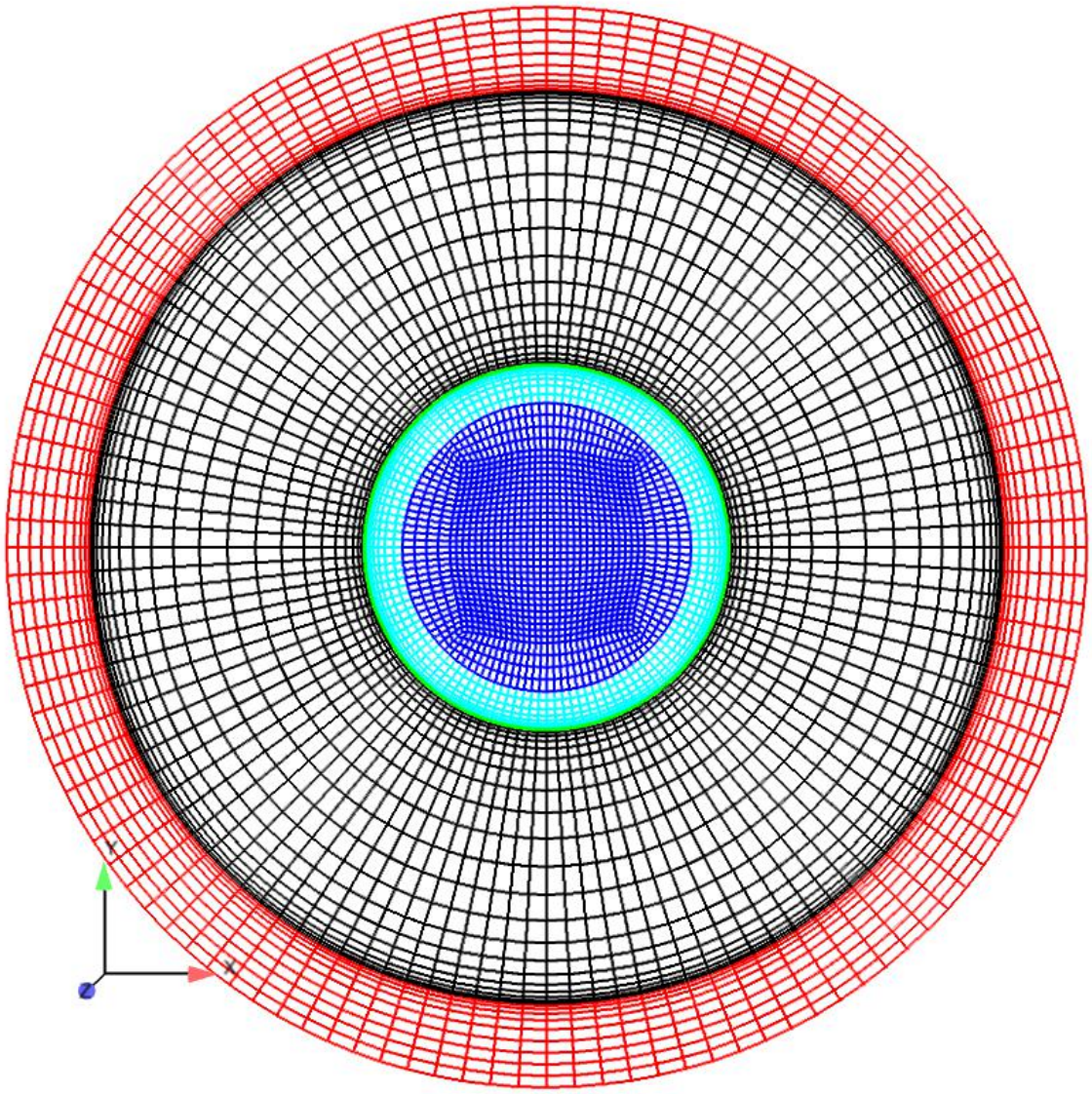

Figure 5. Baseline mesh (8 micron at conductor-dielectric interfaces).

The mesh shown in Fig. 5 is the baseline mesh used for the mesh-refinement results presented in this section. The results compare spatial truncation errors using the two approaches defined in the previous section. The current approach computes the SGEMP direct drive total charge as the difference between the knock-on charge and the induced charge (Turner C. D., 2005)

$$\oint \mathbf{J}_{\beta}(\mathbf{r}) \cdot d\mathbf{s} + \int V(\mathbf{r})\rho(\mathbf{r})d\mathbf{r} \qquad (5.1)$$

In the alternative approach (Drumm, Scrivner, & Hohlfelder, 1991), the results are computed from

$$\int \nabla V(\mathbf{r}) \cdot \mathbf{J}_\beta(\mathbf{r}) d\mathbf{r} \qquad (5.2)$$

where $V(\mathbf{r})$ is a potential function solution of the Poisson equation with boundary conditions of zero on the grounded outer conductor and unity on the loaded inner conductor, and $\mathbf{J}_\beta(\mathbf{r})$ is the electron current distribution in the dielectric provided by the SCEPTRE code. It is essential to perform the integral in Eq. (5.2) as accurately as possible. SCEPTRE uses nodal-based finite elements, so that the solution is computed on the nodes and expanded in the finite-element basis functions to determine the spatial distribution. The integral in Eq. (5.2) is carried out numerically as

$$\sum_{e=1}^{N_{elems}} \sum_{i=1}^{N_{basis}} \sum_{i'=1}^{N_{basis}} V_{e,i} \psi_{e,i',\beta} \int\int \mathbf{\Omega} \cdot \nabla \varphi_i(\mathbf{r}) \varphi_{i'}(\mathbf{r}) d\mathbf{r}\, d\mathbf{\Omega} \qquad (5.3)$$

where $\varphi_i(\mathbf{r})$ are the finite-element basis functions, N_{elems} is the number of elements in the dielectric, N_{basis} is the number of basis functions, $V_{e,i}$ are the nodal values of the potential function, and $\psi_{e,i',\beta}$ are the nodal values of the electron angular flux. The *streaming* matrix elements are precomputed in the SCEPTRE code using quadrature integration for each element as

$$\int \nabla \varphi_i(\mathbf{r}) \varphi_{i'}(\mathbf{r}) d\mathbf{r} \qquad (5.4)$$

Fig. 6 shows the total direct-drive charge computed with both methods, for four levels of mesh refinement from 8 μm to 1 μm, for linear and quadratic quadrilateral finite elements. Use of the current approach with linear elements is quite inaccurate and is off the scale of the graph. The figure shows that for this example problem, accurate results may be obtained with a fairly coarse mesh, especially when using quadratic basis functions. Fig. 7 shows the error in the various calculations compared with the Richardson extrapolated value.

The new method does not include Radiation Induced Conductivity (RIC), but it might be possible to include an approximate RIC model in the future. The radiation transport calculation is performed in steady state, so that it is assumed that the time history of the electron current distribution is the same as that of the source photons. It is further assumed that the time scale of the electrical response is long compared with the redistribution of electrons in the dielectric in the presence of an electric field, so that the electron current distribution provided by SCEPTRE serves as a source term for the EM modeling, but is not modified by the EM modeling. Including RIC lowers direct drive, so neglecting it should at worst provide an upper bound on the result.

Inclusion of RIC would add an additional current term near the boundary layers where the energy deposition is large, which would modify the time history of the direct-drive, and maybe the total direct-drive charge as well. It would be possible to approximate RIC as a perturbation by running SCEPTRE to compute the electron current and energy deposition, model the EM without RIC to compute an approximate electric field, compute an approximate RIC current based on the approximate electric field and energy deposition, and then rerun the EM model with the RIC current added to the SCEPTRE electron current drive. What isn't clear is whether including RIC in this way would require the extremely fine interface meshing that we're trying to avoid with the new method.

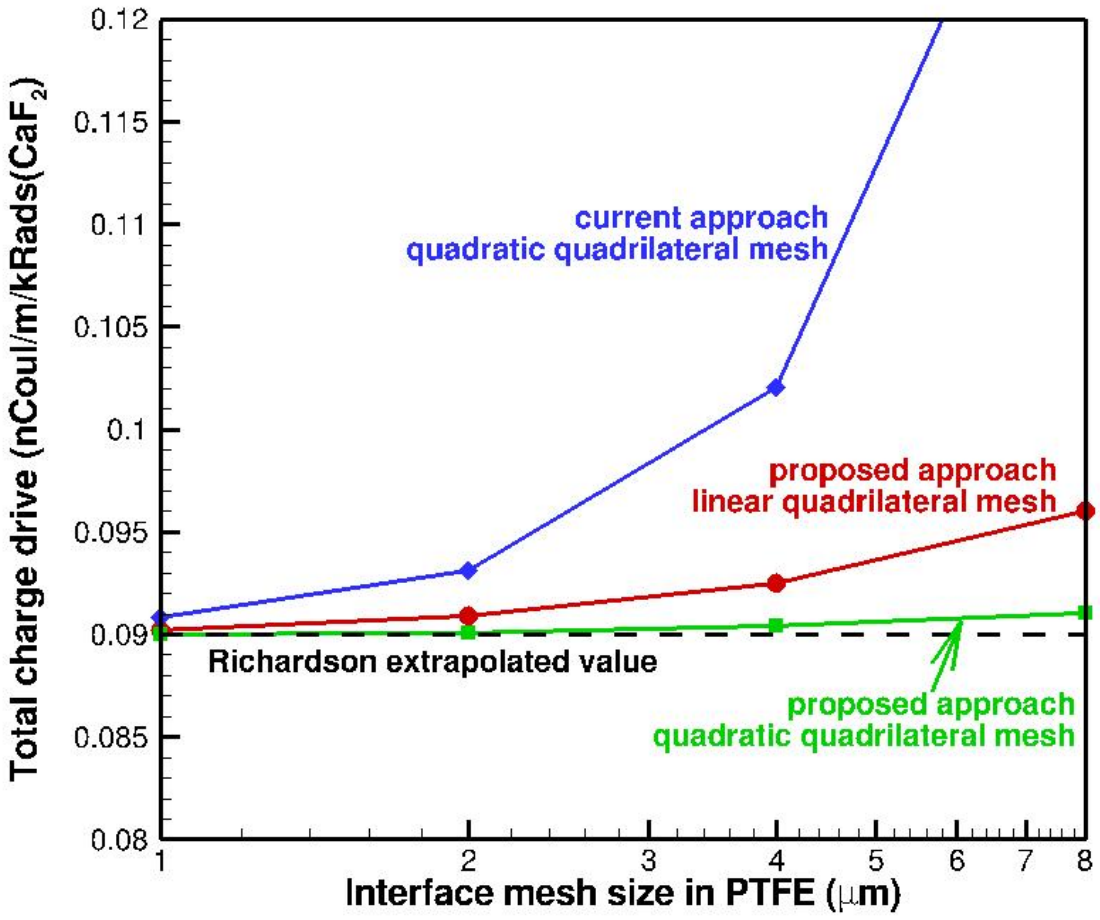

Figure 6. Total direct-drive charge vs. interface mesh size for current and proposed methods.

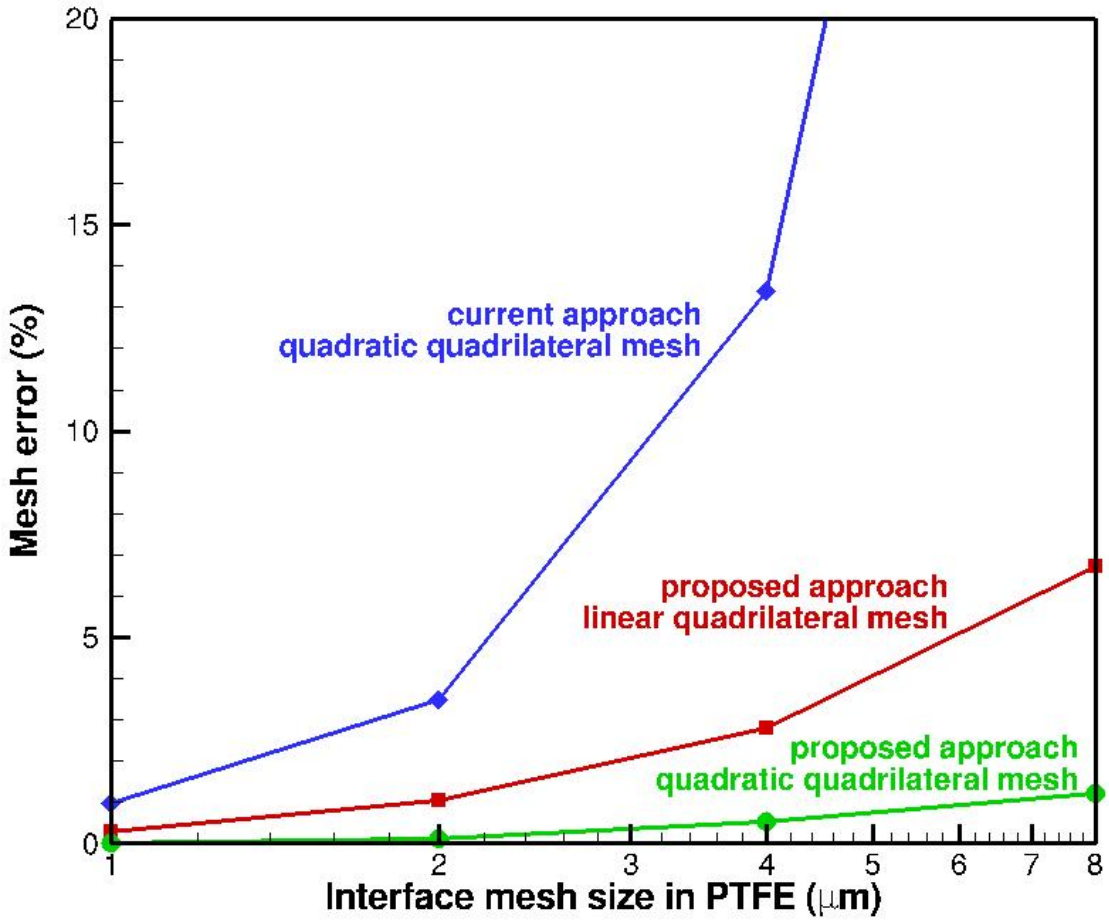

Figure 7. Error in SGEMP total drive charge vs. interface mesh size.

6. ADJOINT CABLE SGEMP MODELING

An adjoint calculation is essentially performed backwards from detector to source, rather than from source to detector (Renken, 1977). An adjoint calculation provides extremely useful information, including the sensitivity of the response (in this case, the cable SGEMP) to the source energy spectrum and angle of incidence.

The first step in performing an adjoint calculation is to compute and adjoint source term. From Eq. (4.8) the SGEMP direct drive response can be computed from the angular electron fluence

$$\mathcal{R} = -\int \vec{\mathcal{E}}(\mathbf{r}) \cdot \mathbf{J}_\beta(\mathbf{r}) d\mathbf{r} = -\iint \boldsymbol{\Omega} \cdot \vec{\mathcal{E}}(\mathbf{r}) \psi_\beta(\mathbf{r}, \boldsymbol{\Omega}) d\mathbf{r} d\boldsymbol{\Omega} \qquad (6.1)$$

where the electron current is related to the angular electron fluence by

$$\mathbf{J}_\beta(\mathbf{r}) = \int \mathbf{\Omega}\psi_\beta(\mathbf{r},\mathbf{\Omega})d\mathbf{\Omega} \qquad (6.2)$$

The forward and adjoint solutions are related to each other by (Renken, 1977)

$$\iint Q_\beta^\dagger(\mathbf{r},\mathbf{\Omega})\psi_\beta(\mathbf{r},\mathbf{\Omega})d\mathbf{r}d\mathbf{\Omega} = \int \oint \psi_\gamma^{bdry}(\mathbf{r},\mathbf{\Omega})\psi_\gamma^{\dagger bdry}(\mathbf{r},\mathbf{\Omega})d\mathbf{s}d\mathbf{\Omega} \qquad (6.3)$$

so that the response may be written in terms of the photon source environment and the adjoint angular fluence at the boundary surface of the cable

$$\mathcal{R} = \int \oint \psi_\gamma^{bdry}(\mathbf{r},\mathbf{\Omega})\psi_\gamma^{\dagger bdry}(\mathbf{r},\mathbf{\Omega})d\mathbf{s}d\mathbf{\Omega} \qquad (6.4)$$

The adjoint electron source is computed from the direction vector and the electric field vector from

$$\begin{aligned} Q_\beta^\dagger(\mathbf{r},\mathbf{\Omega}) &= -\mathbf{\Omega}\cdot\vec{\mathcal{E}}(\mathbf{r}) \quad \text{in dielectric} \\ &= 0 \qquad\qquad\quad \text{in conductor} \end{aligned} \qquad (6.5)$$

Fig. 8 shows the result of an adjoint calculation for a normally-incident source, with a normalized Pithon spectrum superimposed. Fig. 9 adds the adjoint response function for several other angles of incidence. A number of interesting observations may be made in referring to Figs. 8 and 9. Photons with energies less that about 25 keV are stopped by the outer shield and contribute nothing to the cable SGEMP direct drive, so the adjoint response is zero for lower-energy photons. Photons from about 30 keV to 60 keV have sufficient energy to penetrate the outer shield and knock electrons into the dielectric, inducing a negative drive current into the center conductor, but are not able to penetrate the dielectric to reach the center conductor to contribute to a knock-on charge component. As the photon energy increases about 60 keV, photons penetrate the dielectric material into the silver layer, and generate a knock-on charge component that generates a positive direct-drive charge that counteracts the induced charge from electron emission for the outer ground. As the photon energy increases above 60 keV, the electron emission from the center conductor dominates the response. As the photon direction of incidence goes from normally incident to more grazing angles, the direct drive decreases due to greater photon attenuation.

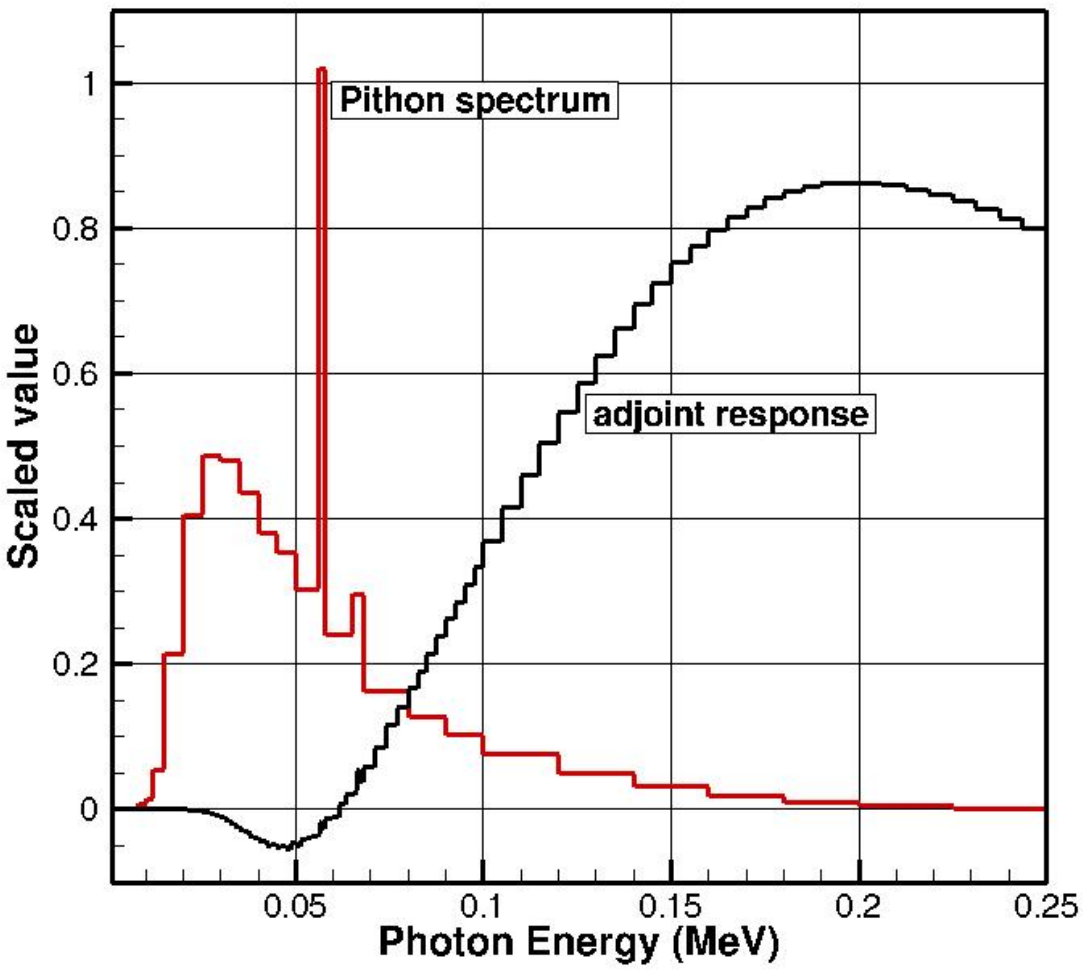

Figure 8. Sensitivity of drive charge to photon source energy for a normally-incident source.

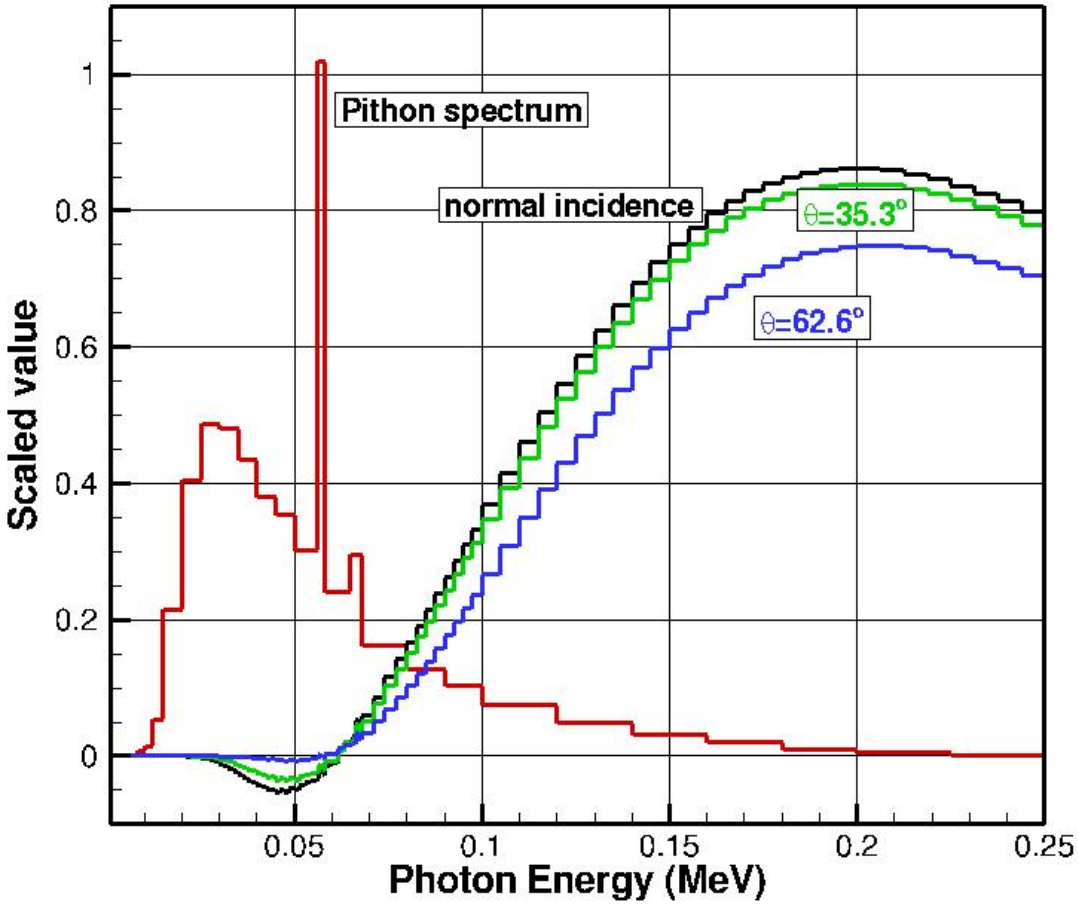

Figure 9. Sensitivity of drive charge to photon energy for several angles of incidence.

7. ENERGY MESH AND ANGULAR QUADRATURE

In this section the effects of changing the electron and photon energy group structure and of changing the angular scattering order and angular quadrature order are investigated. Photon/electron cross sections are obtained from the CEPXS code (Lorence, 1989), which relies upon the analyst to specify an energy-group structure for the photons and electrons, and Legendre angular expansion parameters for the angular scattering approximation. The appropriate energy/angle parameters for x-ray transport may be quite different than that for γ-ray transport, so guidance for x-ray modeling will be included here, and guidance for γ-ray modeling will be included in a subsequent report.

7.1. Energy mesh refinement

One consideration that may be important is the location of the K-edges in any relevant materials in the problem geometry (Kensek, 2014). The reason for this is that the photon attenuation coefficient takes a substantial jump at the K-edge, so an energy group that extends across the K-edge may include significant error in approximating the attenuation coefficient, e.g. the silver attenuation coefficient is shown in Fig. 10. For this problem placing an energy group boundary at the silver K-edge of 25.5 keV would be desirable.

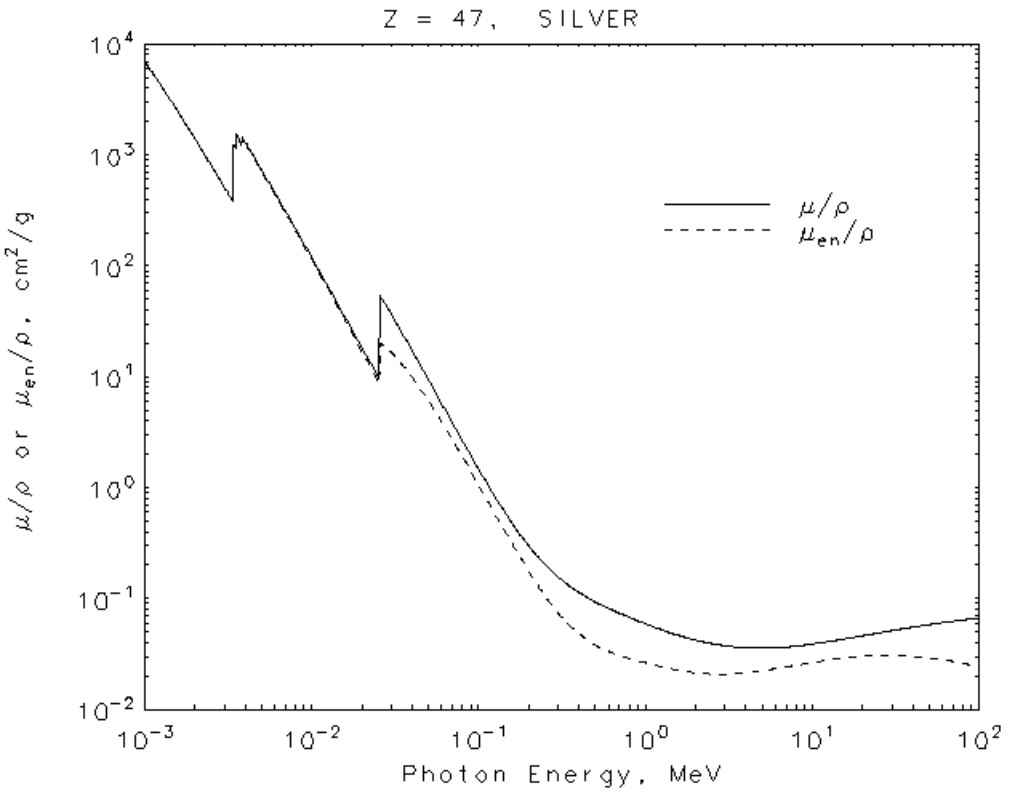

(NIST)

Figure 10. Silver attenuation coefficient vs. photon energy.

Energy groups for a CEPXS calculation may be specified as one of three types, uniform linear distribution, log distribution or user specified boundaries. We compare the SGEMP results here for several levels of refinement of a user specified photon energy group structure, and several levels of refinement for a linear or log electron energy group distribution. In the course of this work a bug in the CEPXS code was discovered that may produce inaccurate results for cases where the electron group width is substantially smaller than the photon group width. This is commonly encountered when using a linear photon group structure with a log electron group structure. We present results for cross section libraries created both before and after the bug fix in the CEPXS code.

The cable SGEMP vs. number of electron energy groups is shown in Fig. 11, which unexpectedly shows the result getting much worse as the number of electron groups is increased. The same data plotted vs. number of electron groups is shown in Fig. 12.

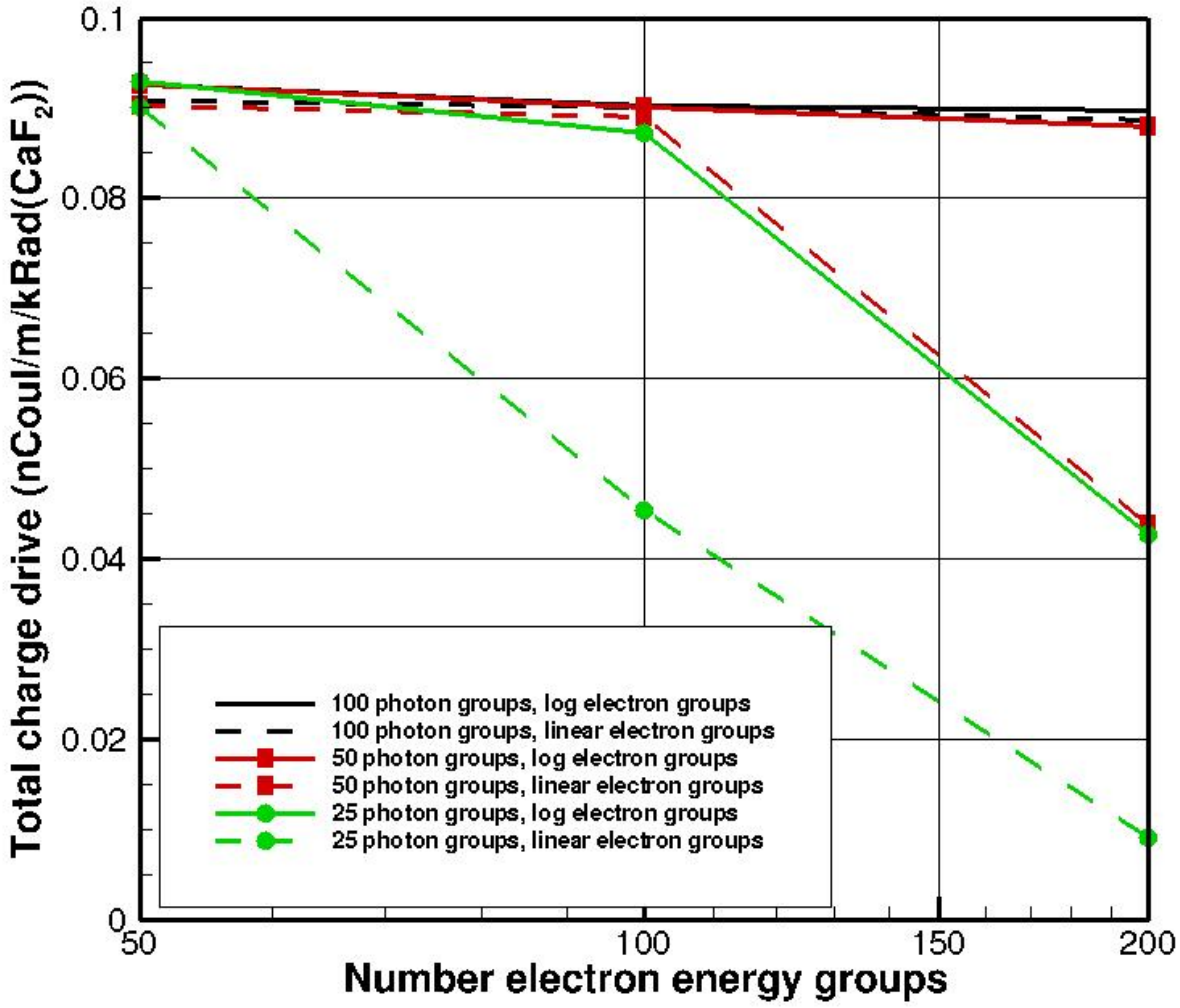

Figure 11. Drive charge vs. number of electron groups before bug fix.

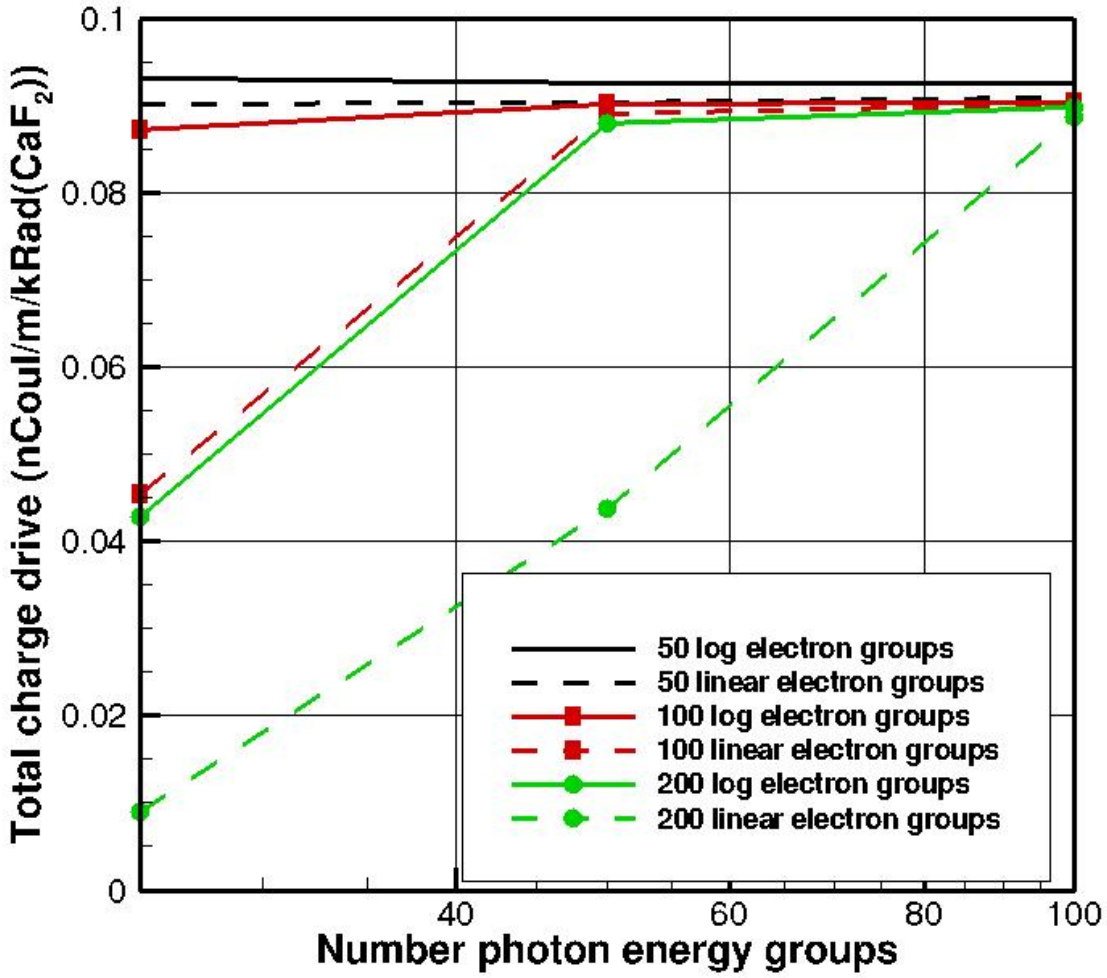

Figure 12. Drive charge vs. number of photon energy groups before bug fix.

The bug is in the processing of the photoelectric cross section, where the Heaviside step function from Eq. VIII.10 (Lorence, 1989) was left out of the integration, resulting in a possible incorrect integration range in computing the photoelectric cross section. After introducing the bug fix (Kensek, 2014) to the integration limits into the code, the results are shown in Figs. 13 and 14, which show much less sensitivity to the number of photon and electron energy groups. The result converges slowly with increasing the number of electron groups, even using second-order accurate energy differencing, and is relatively insensitive to the number of photon groups.

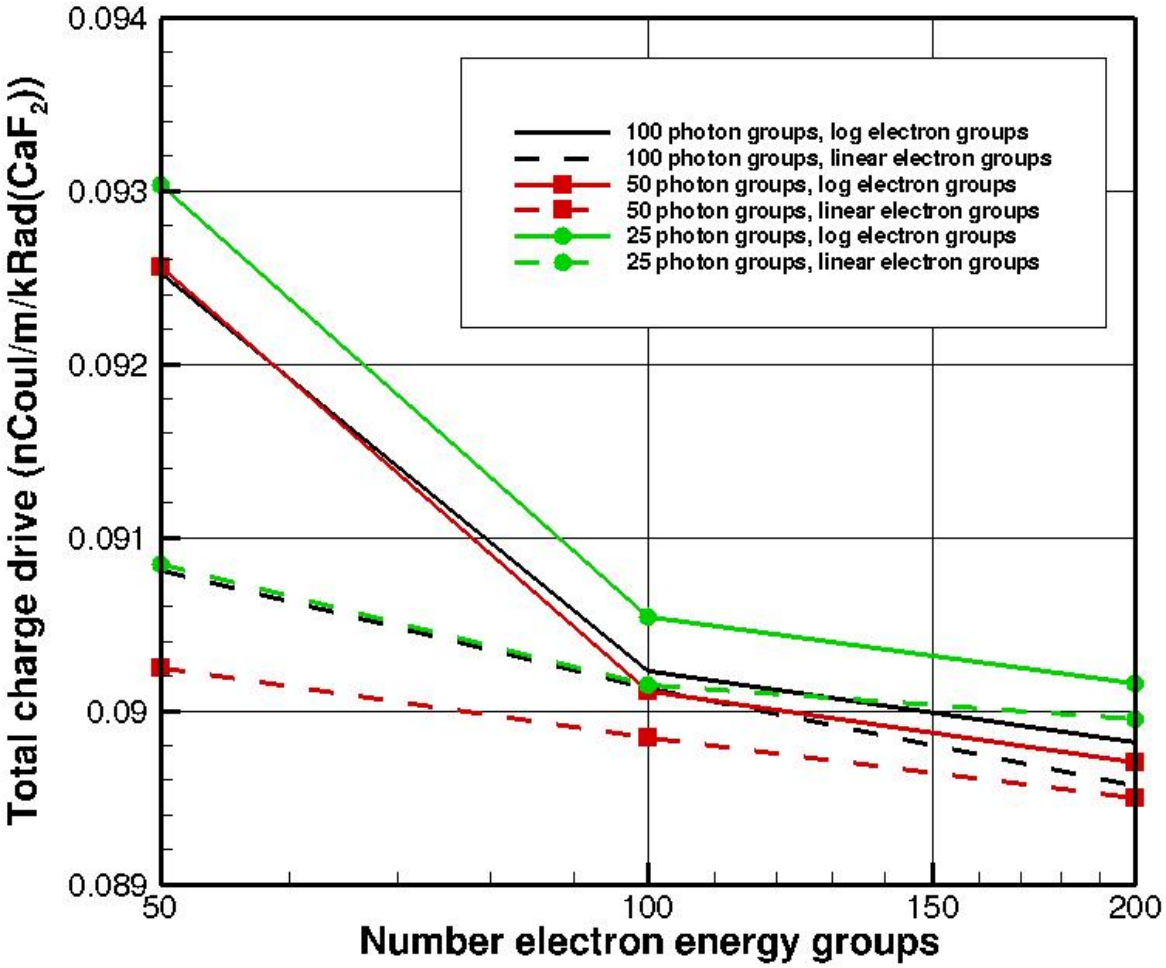

Figure 13. Drive charge vs. number of photon groups after bug fix.

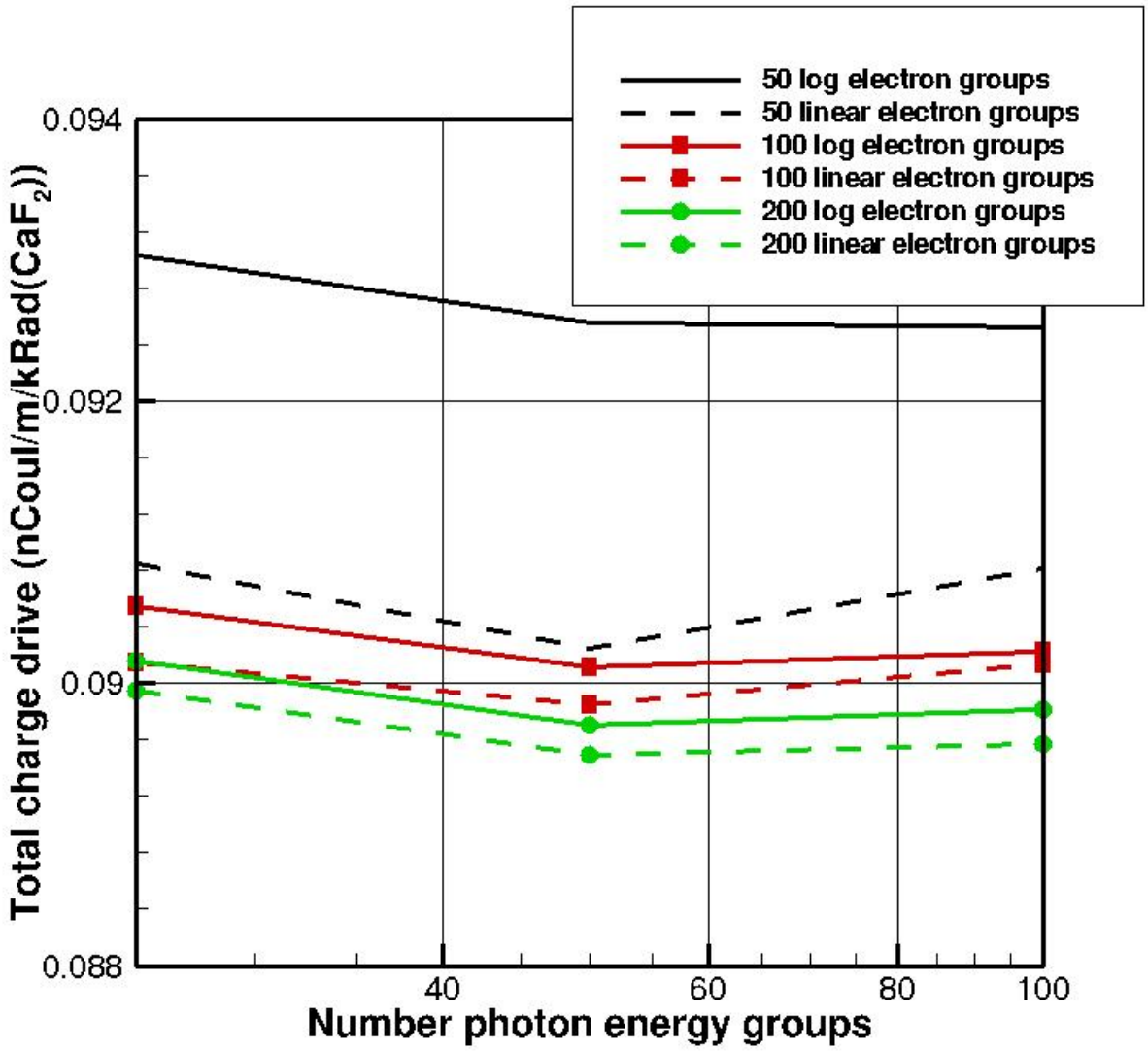

Figure 14. Drive charge vs. number of photon groups after bug fix.

7.2. Angular approximations

The angular approximation used in a transport calculation refers both to the Legendre angular scattering approximation used to model the angular dependence of the photon and electron scattering, and the order of the angular quadrature used to model the angular dependence of the angular flux. SCEPTRE also has a number of specialized algorithms for dealing with the extremely forward-peaked scattering encountered with charged-particle transport.

7.2.1. Scattering order

SCEPTRE has a number of specialized methods for dealing with highly-forward peaked electron scattering. The scattering anisotropy of γ-rays is much more severe than that for x-rays, so that the specialized methods will be more relevant for γ-ray transport, which will be covered in a subsequent report. For neutral-particle transport (photon/neutron) that is mildly anisotropic, a low-order Legendre polynomial approximation is usually sufficient to accurately model the scattering. For low-energy electron transport, a low-order Legendre expansion may be sufficient, but special treatment may be required.

If the Legendre polynomial expansion is not sufficient to accurately model the electron scattering, SCEPTRE has two methods for dealing with extremely anisotropic scattering. One method is to explicitly model a δ-function down scattering term (Drumm C. , 2007). In this approach a δ-function down scattering term is treated explicitly and removed from the scattering cross section, significantly reducing the anisotropy and magnitude of the remaining scattering cross section. This method is effective and maintains the symmetry of the linear system. Most production radiation transport codes compute a down-scatter source from the moments of the angular flux, rather than from the angular flux itself, so this method is not generally available in other transport codes.

Another approach is to use a Galerkin scattering treatment (Morel, 1989). This is the approach that is used in the one-dimensional CEPXS/ONELD and ADEPT codes. In the Galerkin approach, a square moment-to-discrete matrix is constructed that is invertible, so that the conversion from discrete space to moment space and back again is exact. For one-dimensional geometry, the use of Gauss-Legendre quadrature with the same number of Legendre moments as discrete directions is Galerkin. For multi-dimensional geometries, the Galerkin scattering treatment is not unique, but the procedure is the same. A square, invertible moment-to-discrete matrix is constructed, which is able to exactly handle the δ-function down scatter. SCEPTRE contains algorithms for computing Galerkin moment-to-discrete matrices for all available quadrature types, level-symmetric, Lebedev, Gauss-Legendre, and Lobatto.

Results for all three options are presented here, providing some guidance on the order of scattering needed for accurate modeling. Fig. 15 shows the cable SGEMP direct drive vs. Legendre scattering order for each of the three methods described above. The δ-function down scattering method and Galerkin scattering methods provide essentially identical results and are very accurate even for low scattering order. Using a standard Legendre polynomial expansion is acceptably accurate if the angular quadrature order is sufficient to model the angular dependence of the Legendre polynomials.

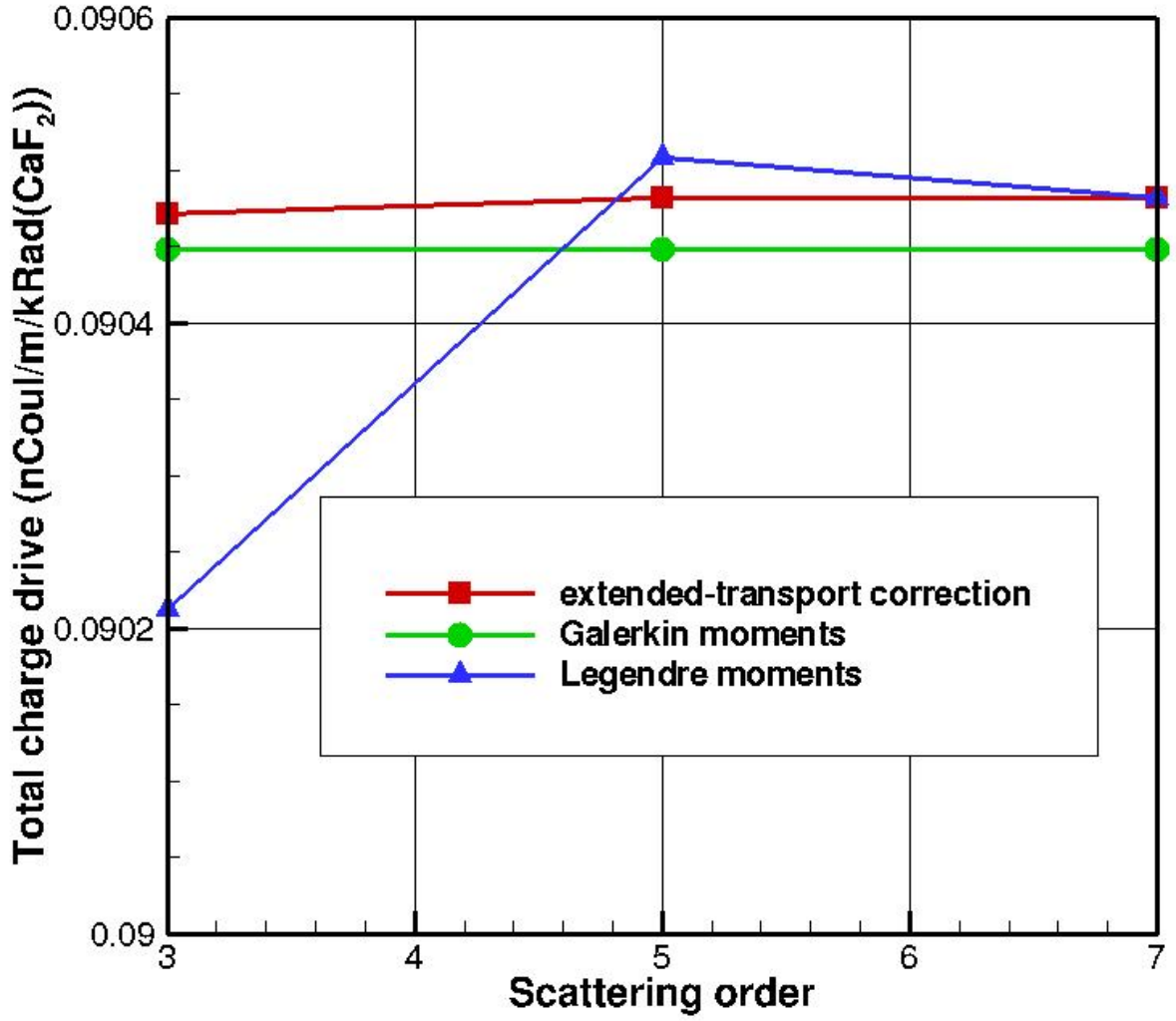

Figure 15. Drive charge vs. scattering order.

7.2.2. Angular quadrature

SCEPTRE contains two built-in quadrature sets for multidimensional geometries: 1) level-symmetric, and 2) Lebedev. Lebedev has several advantages relative to the level-symmetric set. Higher-order quadrature sets are available with Lebedev (level-symmetric quadrature sets begin have negative weights around order 20, while Lebedev quadrature sets are available for order up to 130). Lebedev quadrature sets generally have fewer discrete directions for comparable accuracy, and Lebedev quadrature sets have directions along the Cartesian coordinate axes, which is convenient for modeling normally-incident sources. The cable SGEMP direct drive vs. angular quadrature order is shown in Fig. 16, using the δ-function scattering treatment, showing that the cable SGEMP is fairly insensitive to the angular scattering order for x-ray transport.

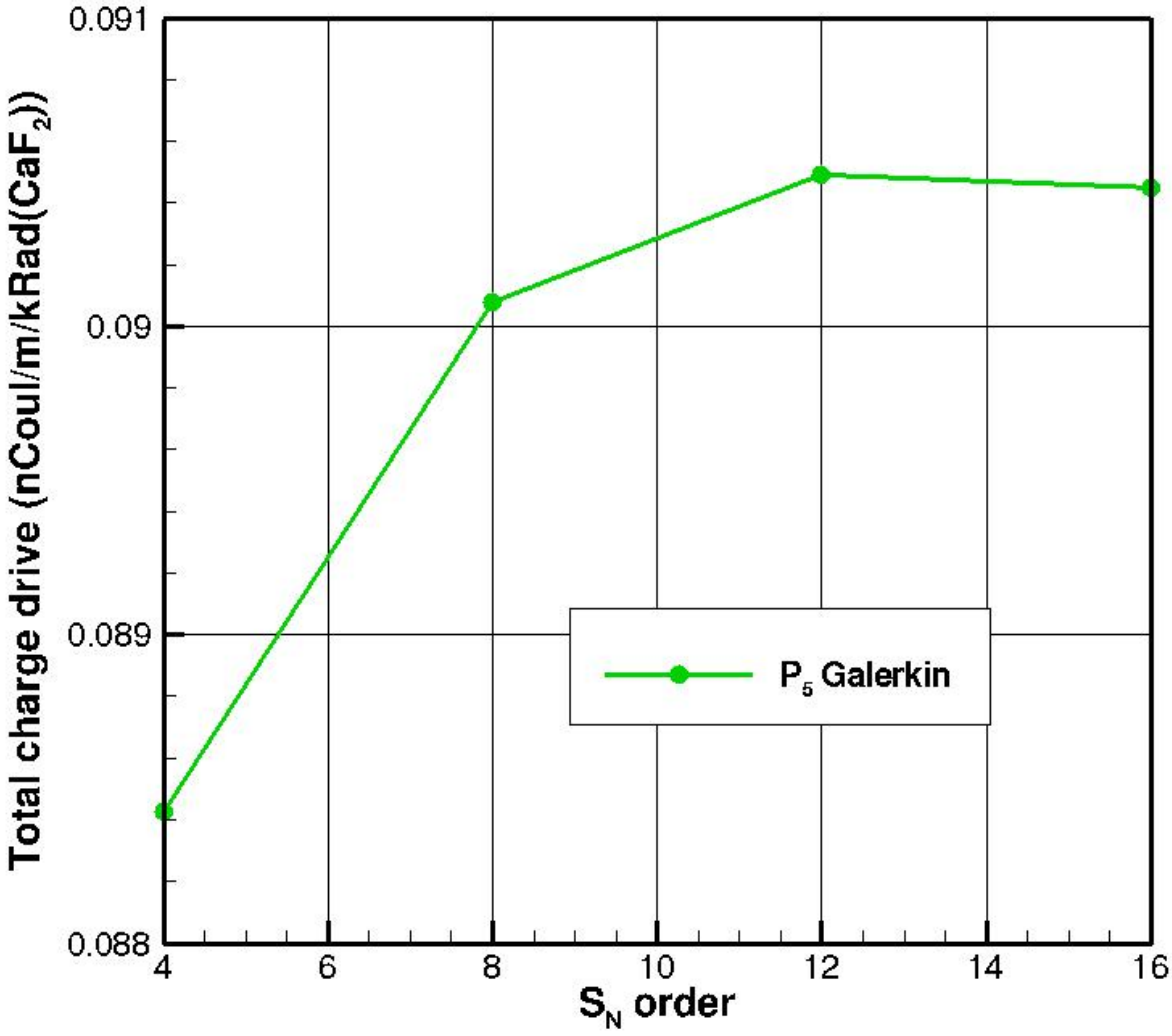

Figure 16. Drive charge vs. angular quadrature order.

8. COMPARISON OF SCEPTRE SOLVER METHODS

The SCEPTRE code has several different solution algorithms available, and the user can select on a group-by-group basis which algorithm to use. The reason for having a variety of algorithms available in the code is that, due to differences in the cross sections, the iterative convergence rates of the various groups may be very different. It has been found that using different algorithms for the different particle types and differing energies results in improved overall performance. SCEPTRE has a state-of-the art sweeps based solver, commonly used by most neutron/gamma transport codes, which is optimal for x-ray/γ-ray transport (Lewis & Miller, 1984). For charged-particle transport, however, the convergence of the sweeps-based solver may be slow due to the large scattering ratio of charged-particle cross sections.

In addition to the sweeps-based solver, SCEPTRE has a class of algorithms based on an entirely different solution approach with very different solution properties. In the sweeps solver, the scattering source term is included with the other source terms on the right hand side of the equation. In this approach, the solution for each particle direction is determined independently, and the scattering source term is updated until convergence. With the alternative algorithm, the scattering source term is included with the streaming and removal operators on the left hand side of the equation, so that spatial and angular dependences of the solution are solved simultaneously. The main drawback of this method is that the memory requirement may be large, but if enough memory is available, this method is a useful alternative to the sweeps solver that generally converges more efficiently for charged particles. In this approach, the linear system is constructed and handed off to Trilinos (Heroux & Willenbring, 2003) for solution using one of the Krylov iterative methods available in the Trilinos package.

SCEPTRE includes the capability of solving several different forms of the Boltzmann transport equation. Furthermore, SCEPTRE has the option of using either Discontinuous Finite Elements (DFE) or Continuous Finite Elements (CFE). Use of DFE tends to be more accurate for certain transport problems but is also more expensive.

One of the forms of the transport equation that SCEPTRE uses is called the Self-Adjoint Angular Flux (SAAF) algorithm (Morel J. , 1999) that performs well for may applications. This method is based on a second-order form of the Boltzmann equation and uses CFE, resulting in a Symmetric Positive Definite (SPD) linear system, so that the highly-efficient Krylov Conjugate Gradients (CG) iterative method is applicable. SCEPTRE also has a Least-Squares (LS) algorithm, which is based on the first-order Boltzmann equation and uses CFE, also resulting in an SPD linear system. Based on limited experience to date, the LS method tends to be less accurate than other methods, but more experience is needed to draw any conclusions about the method. SCEPTRE also has a method based on the first-order Boltzmann equation, making use of DFE. This method produces a linear system that is not SPD, so that the CG algorithm is not applicable. One of the other algorithms available in Trilinos, such as Generalized Minimum RESidual (GMRES), may be used.

By using Trilinos to perform the iterative linear solve, it is fairly easy to include various preconditioiners in the algorithm. SCEPTRE includes options for three different preconditioners, 1) an incomplete-factorization method, 2) a multi-level method, and 3) a SCEPTRE-specific preconditioner using the diagonals of the blocks in the system matrix as a preconditioner. It generally takes some experimentation to determine which combination of solvers and preconditioners is optimal for a given application and particle/energy group.

Fig. 17 compares the accuracy of the DFE method based on the first-order Boltzmann equation with the SAAF method using CFE elements for both linear and quadratic elements. The two methods have about the same accuracy, but the first-order DFE method over predicts, while the SAAF CFE under predicts the result. Fig. 18 compares the accuracy of the LS CFE algorithm with the first-order DFE method, showing the LS algorithm less accurate that the first-order DFE method.

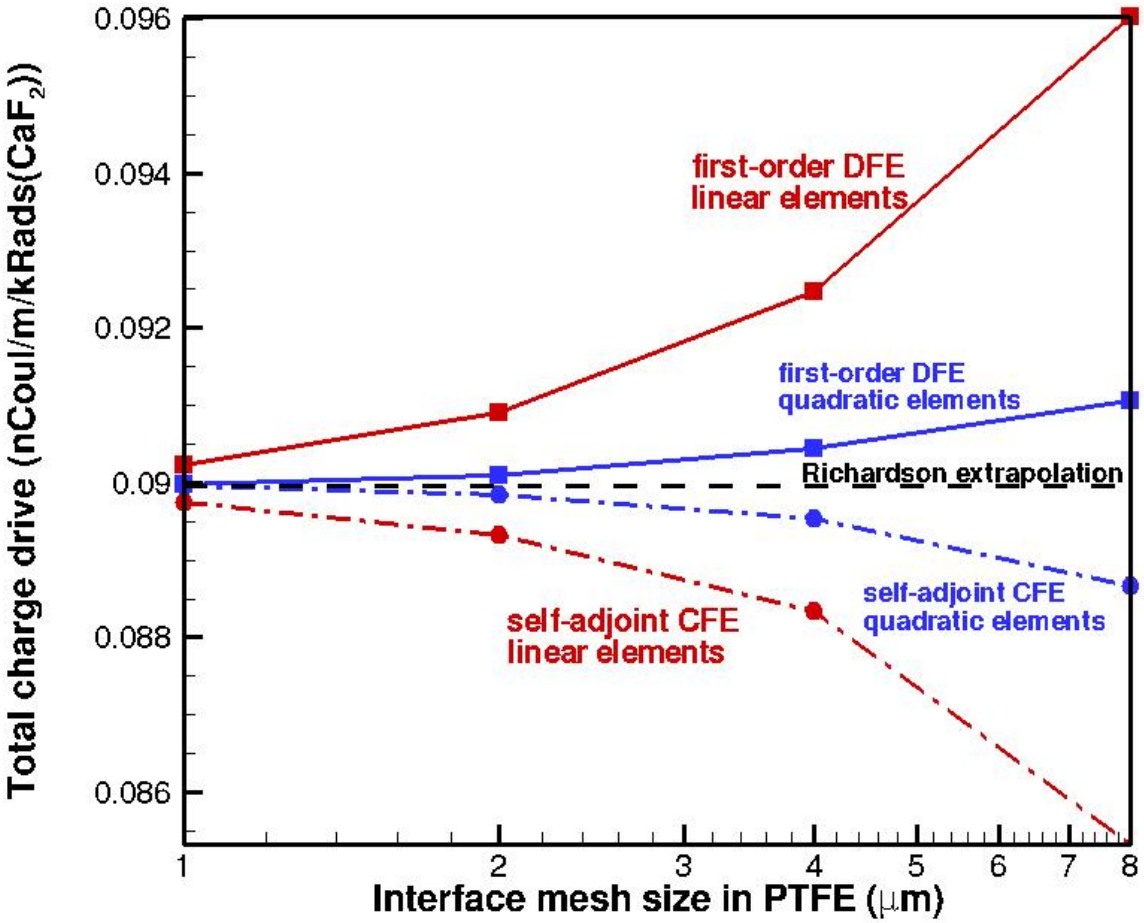

Figure 17. Comparison of spatial convergence of DFE and self-adjoint CFE methods.

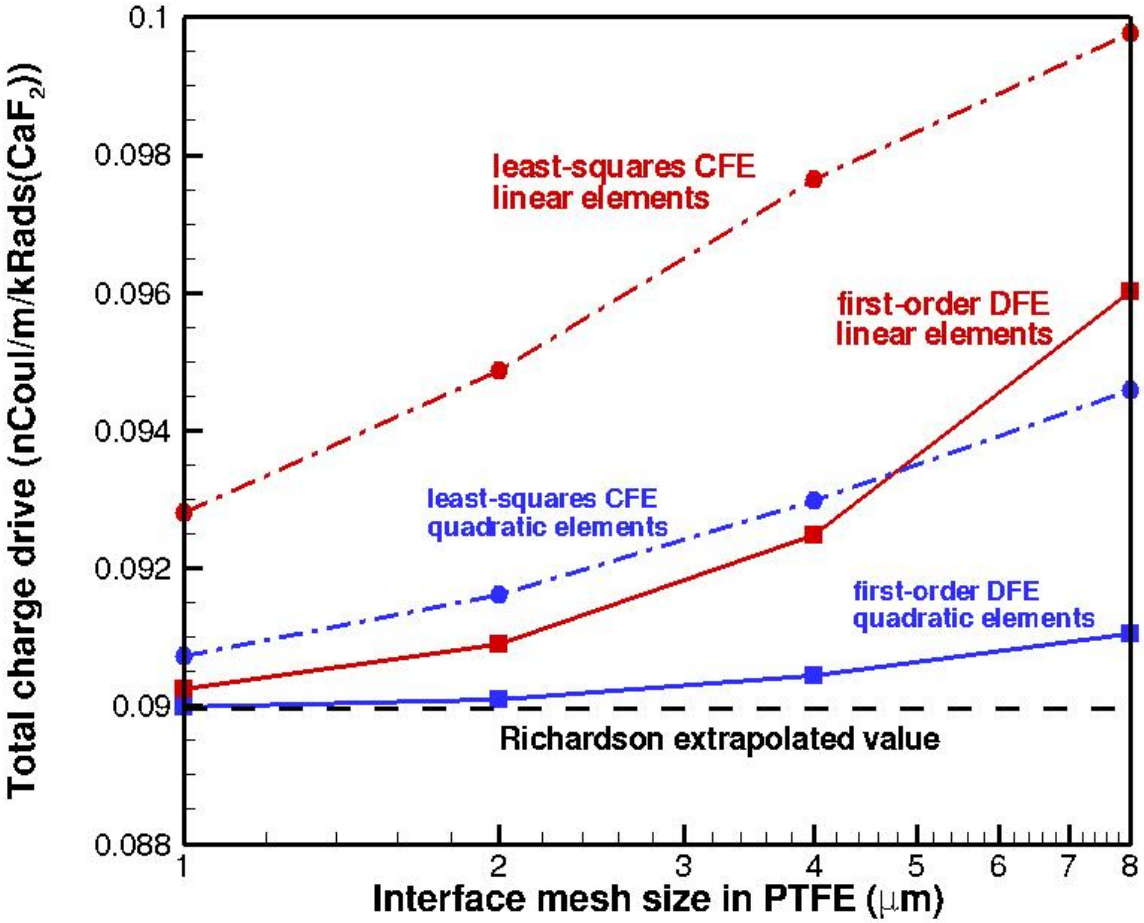

Figure 18. Comparison of spatial convergence of DFE and least-squares CFE methods.

Fig. 19 compares solver times for the various algorithms. A first-order DFE sweeps-based algorithm is used for the photon energy groups for all cases. For the electron groups, three different Krylov algorithms are compared. The first-order DFE Krylov algorithm converges to the same solution as the first-order sweeps based algorithm, but is the slowest of the Krylov algorithms. An incomplete-factorization preconditioner is used for this test. The two CFE algorithms are both faster than the DFE algorithm, with the SAAF performing better than the LS algorithm, so the SAAF algorithm outperforms the LS method in both accuracy and efficiency.

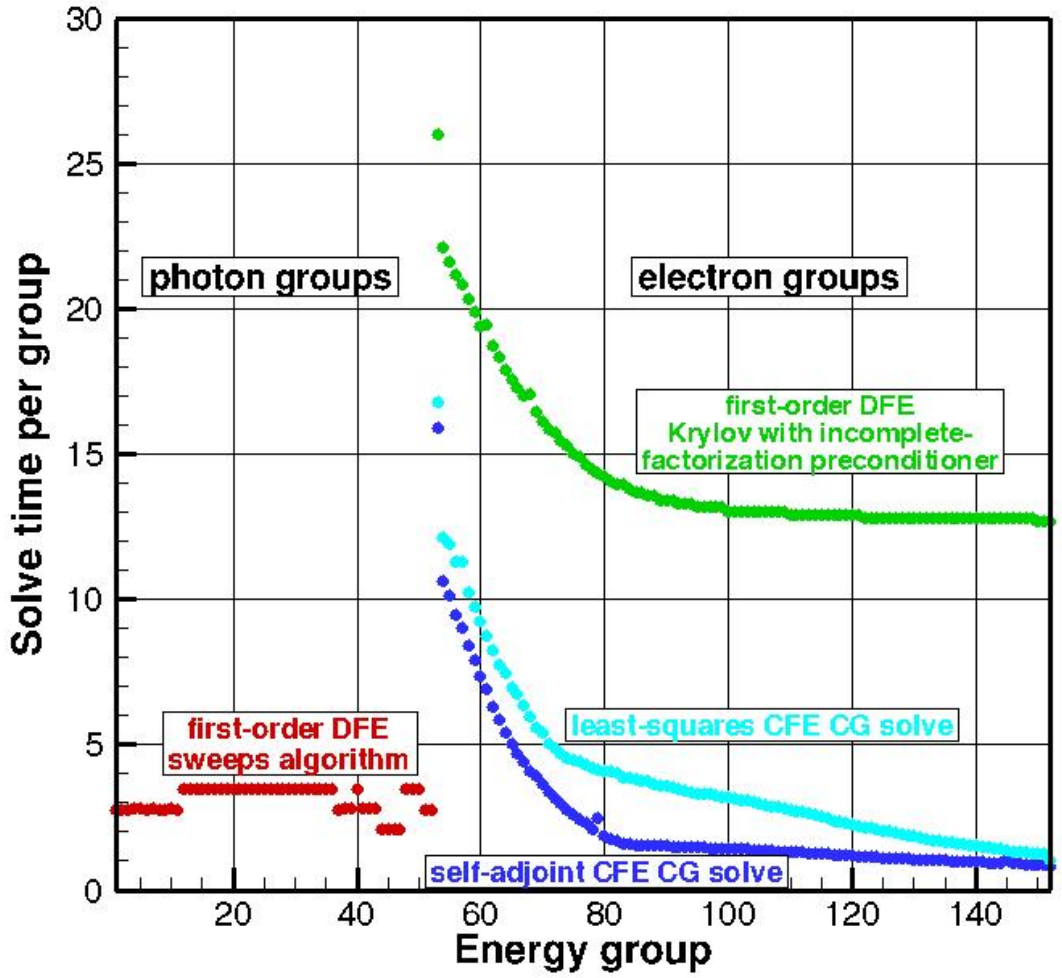

Figure 19. Solver time comparison of various algorithms.

9. CONCLUSIONS AND SUMMARY

This report has summarized experiences gained by the authors in performing radiation-transport analyses for cable SGEMP with the SCEPTRE radiation transport code. We have investigated the effect of refining the spatial, energy and angular approximations to provide some guidance on appropriate starting values to use for typical x-ray SGEMP analysis. Starting with a one-dimensional model and observing the spatial dependence of the solution near material interfaces provides useful guidance in creating a baseline spatial mesh. It is essential to perform some refinement of the spatial mesh, energy group structure and angular quadrature to ensure that the solution is converging as expected.

We have provided preliminary results for an alternative formulation of the SGEMP problem that is relatively insensitive to the spatial mesh refinement near material interfaces. Based on the limited experience presented here, the method seems sound, but additional testing is necessary to establish confidence in the method. Further development would be required if it is necessary to include a RIC model with this method.

We have also presented the results of an adjoint calculation, demonstrating the utility of adjoint modeling for revealing the sensitivity of the SGEMP drive current to source energy and angle of incidence.

REFERENCES

Drumm, C. (2007). An Analysis of the Extended-Transport Correction with Application to Electron Beam Transport. *Nuclear Science and Engineering*, 355-366.

Drumm, C. R., Scrivner, G. J., & Hohlfelder, J. J. (1991). Compton Diode and Coaxial Cable Response to Gamma Irradiation. *Advanced in Mathematics, Computations, and Reactor Physics* (pp. 7.2.3.1-7.2.3.14). Pittsburgh: American Nuclear Society.

Heroux, M. A., & Willenbring, J. M. (2003). *Trilinos Users Guide.* Albuquerque: Sandia National Laboratories report, SAND2003-2952.

Kensek, R. P. (2014). private communication.

Lewis, E. E., & Miller, W. F. (1984). *Computational Methods of Neutron Transport.* New York: John Wiley & Sons.

Lorence, L. J., Morel, J. E., & and Valdez, G. D. (1989). *Physics Guide to CEPXS: A Multigroup Coupled Electron-Photon Cross-Section Generating Code Version 1.0.* Albuquerque, NM 87185: SAND89-1685 Sandia National Laboratories.

Morel, J. (1989). A Hybrid Collocation-Galerkin-Sn Method for Solving the Boltzmann Transport Equation. *Nuclear Science and Engineering*, 72-87.

Morel, J. E., & McGhee, J. M. (1999). A Self-Adjoint Angular Flux Equation. *Nuclear Science and Engineering*, 312-325.

NIST. (n.d.). Retrieved from http://physics.nist.gov/PhysRefData/XrayMassCoef/ElemTab/z47.html

Pautz, S., Bohnhoff, W., Drumm, C., & Fan, W. (2009). Parallel Discrete Ordinates Methods in the SCEPTRE Radiation Transport Project. *International Conference on Mathematics, Computational Methods & Reactor Physics (M&C 2009)* (pp. 1-12). Saratoga Springs, New York: American Nuclear Society.

Renken, J. H. (1977). Determination of the Probing Distance in Pulsed-Neutron Uranium Logging Experiments. *Nuclear Science and Engineering*, 330-335.

Riordan, J. (2008, August). Pithon Reflex Triode Spectra. *private communication.*

Shockley, W. (1938). Currents to Conductors Induced by a Moving Point Charge. *Journal of Applied Physics*, 635-636.

Turner, C. D. (2005). *EMPHASIS/Nevada CABANA.* Albuquerque, New Mexico 87185: Sandia National Laboratories report, SAND2005-1107.

Turner, C. D., Pasik, M. F., & Seidel, D. B. (2011). *EMPHASIS/Nevada UTDEM.* Albuquerque, New Mexico 87185: Sandia National Laboratories report, SAND2011-6644.

DISTRIBUTION

1	D. T. Blackfield LLNL P. O. Box 808 Livermore, CA 94551		
1	MS 1152	C. D. Turner	1352
1	MS 1152	K. Cartwright	1352
1	MS 1167	E. F. Hartman	1343
1	MS 1167	R. Romero	1343
1	MS 1167	T. J. Sheridan	1343
1	MS 1167	T. A. Zarick	1343
1	MS 1168	B. V. Oliver	1352
1	MS 1179	W. J. Bohnhoff	1341
1	MS 1179	C. R. Drumm	1341
1	MS 1179	W. C. Fan	1341
1	MS 1179	B. C. Franke	1341
1	MS 1179	R. P. Kensek	1341
1	MS 1179	T. W. Laub	1341
1	MS 1179	L. J. Lorence	1341
1	MS 1179	S. D. Pautz	1341
1	MS 0899	Technical Library	9536 (electronic copy)


Sandia National Laboratories